ADVANCED ENERGY MATERIALS
www.advenergymat.de

Atomic Layer Deposited Aluminum Oxide for Interface Passivation of $Cu_2ZnSn(S,Se)_4$ Thin-Film Solar Cells

*Yun Seog Lee, Talia Gershon, Teodor K. Todorov, Wei Wang, Mark T. Winkler, Marinus Hopstaken, Oki Gunawan, and Jeehwan Kim**

Kesterite $Cu_2ZnSn(S,Se)_4$ (CZTS) represents an attractive class of semiconductor materials with a suitable bandgap (E_g) range (1–1.5 eV) for low-cost and scalable next-generation photovoltaics (PV). Much of the CZTS solar cell device architecture is adopted directly from $Cu(In,Ga)Se_2$ (CIGS)-based photovoltaic technology, where typical devices utilize a Mo bottom electrode, a chemical bath deposited CdS buffer layer, and a transparent conducting oxide (TCO) stack of indium tin oxide (ITO)/ZnO, deposited by sputtering.[1] CZTS solar cell devices with the record power conversion efficiency contain the same buffer and TCO stack.[2,3] In contrast to CIGS solar cells, however, CZTS devices suffer from an open-circuit voltage (V_{OC}) deficit (and therefore limited efficiencies), where the measured value is significantly lower than the theoretical maximum. Much of this V_{OC}-deficit ($E_g/q - V_{OC}$, q is the electron charge) has been attributed largely to bulk defects and disorder in the CZTS thin films, which causes local fluctuations of the bandgap and/or the band edges due to locally varying electrostatic potential differences.[4]

An open question remains to what extent the device performance could be improved by passivating defects at various interfaces in the device: the heterojunction, the buffer/TCO interface, and at the grain boundaries of polycrystalline CZTS thin films. Atomic layer deposition (ALD), a process involving highly reactive organo-metallic precursors, e.g., trimethyl-aluminium (TMA), is known to provide excellent passivation by reacting with the surface defects of compound semiconductor materials.[5–7] In addition, the ALD process enables conformal coverage of the metal oxide on cracks, trenches, and pinholes with high aspect ratios and complex geometries.[7] These types of structural defects have been identified as problematic in solution-processed CZTS thin films, and frequently lead to detrimental shunting pathways that limit the V_{OC}, the fill factor (FF), and the collection length of photo-generated carriers in the solar cell devices.[8–11]

Dr. Y. S. Lee, Dr. T. Gershon, Dr. T. K. Todorov, Dr. W. Wang, Dr. M. T. Winkler, Dr. M. Hopstaken, Dr. O. Gunawan, Dr. J. Kim
IBM Thomas J. Watson Research Center
Yorktown Heights
NY 10598, USA
Prof. J. Kim
Department of Mechanical Engineering
Department of Materials Science and Engineering
Research Laboratory of Electronics
Massachusetts Institute of Technology
Cambridge, MA 02139, USA
E-mail: jeehwan@mit.edu

DOI: 10.1002/aenm.201600198

Previous studies have reported on several factors that impact surface recombination and passivation in CZTS thin films. For example, secondary phases can either suppress (e.g., ZnS) or exaggerate (e.g., SnS) CZTS surface and grain boundary recombination due to the combined electronic and structural effects of the bandgap and crystal structure incompatibility.[12,13] Etching the CZTS surface in KCN has been found to increase the minority carrier lifetime, presumably by decreasing interfacial recombination.[14] This procedure has been shown to remove some secondary phases and excess chalcogen on the surface. The sulfur-to-selenium chalcogen ratio in the absorber also appears to impact the extent of recombination at the absorber/buffer interface.[15] This was believed to be due to changes in the absorber-buffer band alignment due to the impact of the chalcogen ratio on the absorber bandgap. Additionally, the incorporation of sodium into CZTSSe thin films has been found to passivate surfaces and defects.[16,17] This effect may be related to the formation of wide-bandgap insulating surface oxides which suppress recombination through surface states.[18,19] Most pertinent to the present study, a recent publication showed that a thin Al_2O_3 layer with nanometer-scale openings placed between CZTS and the Mo bottom electrode could help passivate recombination at this rear interface.[20] Thus, we examine the utilization of an Al_2O_3 layer to passivate other interfaces in the device.

In this Communication, we demonstrate that implementing nanometer-scale Al_2O_3 thin films grown by ALD is an effective interface-passivation strategy for improving CZTS solar cell device performance. First, we deposit Al_2O_3 thin films on the CZTS absorber layer to examine passivation of the absorber/buffer interface. Second, we replace the ZnO layer in the ITO/ZnO bilayer TCO stack (on top of the buffer) with an ALD-Al_2O_3 thin film, to mitigate damage to the CdS surface induced by the aggressive bombardment with charged species during TCO stack sputtering processes.[21,22] We show that together these types of ALD-Al_2O_3 layers improve the V_{OC}, FF, long-wavelength collection efficiency, and the short-circuit current density (J_{SC}) of the CZTS solar cell device, resulting in enhanced power conversion efficiencies. Photoluminescence characterization indicates that such enhancements originate, at least in part, from improved interface quality of CZTS devices.

Polycrystalline CZTS thin films are prepared by a hydrazine-based solution process, followed by annealing under chalcogen-rich ambient at over 550 °C for grain coarsening. Per our baseline process, all of the absorber layers undergo "air-annealing" (AA) (annealing for 10 min at 290 °C under ambient conditions) prior to any ALD-Al_2O_3 treatments. TMA, H_2O vapor, and high-purity N_2 gas were used as Al, O sources, and a carrier gas, respectively, for the ALD synthesis of the Al_2O_3 layer. The growth rate of ALD-Al_2O_3 thin films was ≈0.11 nm cycle^{-1}. The

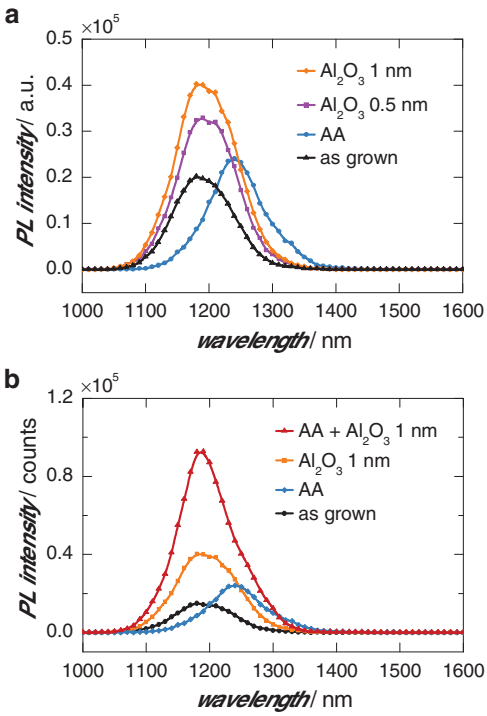

Figure 1. a) PL spectra of CZTS thin-film samples with a various passivation process: 1 nm thick ALD-Al_2O_3 (orange), 0.5 nm thick ALD-Al_2O_3 (purple), AA (blue), and as-grown control sample (black). b) Addition of the PL spectra of CZTS thin-film sample with AA and ALD-Al_2O_3 passivation processes (red), showing additive improvements by the two processes.

substrate temperature was maintained at 150 °C during the ALD process.

It has been reported previously that the photoluminescence (PL) of CZTS increases after subjecting the absorber to AA;[18] it has been proposed that the native oxide formed during AA passivates non-radiative recombination in CZTS, and this step is therefore used in our baseline process for high-efficiency CZTS photovoltaics.[2,3,18,23,24] The PL improvement offered by the AA is readily seen in **Figure 1**a, where the blue curve representing the AA sample has a higher PL peak intensity than the as-grown sample (control) without an Al_2O_3 coating. Interestingly, we observe a shift in the peak position to longer wavelengths after air anneal, which is currently the subject of intense investigation.[25,26] We shall focus on the PL intensity, as it is more directly related to radiative versus non-radiative recombination differences.

Overlaid on the same plot (Figure 1a) are spectra from identical absorber samples that have been coated with 0.5 and 1 nm thick layers of ALD-Al_2O_3. Layers of only 1 nm of Al_2O_3 are found to passivate the CZTSSe surface significantly better than the air-annealing process alone, with respect to non-radiative recombination. In Figure 1b, these same curves are compared with a sample which has been air-annealed prior to deposition of 1 nm of ALD-Al_2O_3. This sample has the overall highest PL intensity by approximately a factor of 2, indicating that the improvements offered by the two processes seem to be additive. In the remainder of the paper, the samples receiving both AA and ALD-Al_2O_3 processing will be compared against our "baseline" material, which has been air-annealed only.

Figure 2a shows a scanning electron microscopy (SEM) image of the standard CZTS solar cell structure presented in

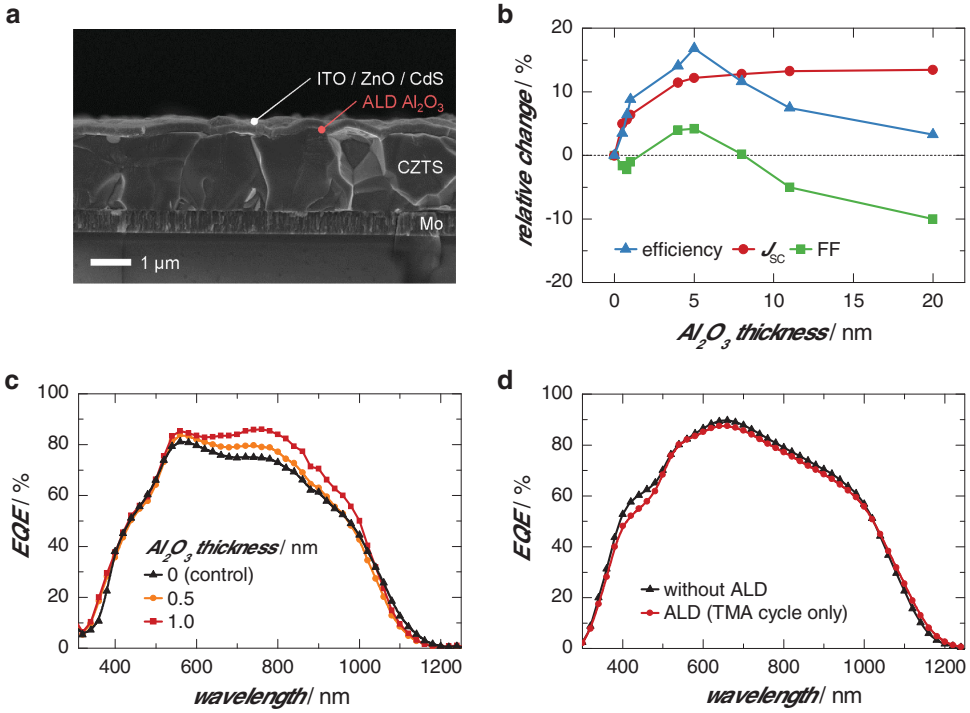

Figure 2. a) Schematic of ALD Al_2O_3 passivation strategies examined in this work. Al_2O_3 layers are examined in between the CdS layer and the sputtered ITO layer, as well as in between the CZTS and the CdS layer. b) Relative changes to the efficiency (blue), J_{SC} (red), and FF (green) of the devices as a function of the starting Al_2O_3 layer thickness. c) EQE spectra from devices containing 0 (black), 0.5 (orange), and 1 nm (red) of ALD-Al_2O_3 between the CZTS and CdS layers. d) EQE spectra from a device without ALD process (black) and a device with TMA-cycle-only ALD process (red).

this study, consisting of a TCO stack (ITO/ZnO), a CdS buffer layer, a CZTS absorber layer (in some cases coated with ALD-Al_2O_3), a Mo bottom electrode layer, and a glass substrate. The effects of the ALD-Al_2O_3 layer thickness on the efficiency, J_{SC}, and FF of the solar cell devices are shown in Figure 2b. As the thickness of the ALD-Al_2O_3 layer deposited between CZTS and CdS increases from 0 to 10 nm, the J_{SC} improves by over 10% and the FF improves by ≈5%, resulting in an overall efficiency improvement of 15%. Above this thickness, the FF and efficiency values decrease, likely due to increased series resistance in the solar cell.

The improved J_{SC} is further analyzed by external quantum efficiency (EQE) measurements. Figure 2c displays the EQE spectra from three CZTS devices prepared with ALD-Al_2O_3 thickness of 0, 0.5, and 1 nm inserted between the CZTS and the CdS layers. The EQE is improved at all wavelengths, and especially in the long-wavelength (>500 nm) region. The EQE improvement in the long-wavelength region indicates an improvement in the collection length of photo-generated carriers, likely due to passivation of the CZTS surface and/or grain boundaries by the ALD-Al_2O_3 layer. To isolate any possible effects from the TMA precursor or the substrate heating in vacuum, a modified ALD-Al_2O_3 process is also examined, where the H_2O vapor pulse cycles were omitted from the standard ALD-Al_2O_3 process, thereby exposing the CZTS layer only to the TMA vapor pulse cycles and the 150 °C process temperature. As displayed in Figure 2d, the TMA vapor treated device shows no significant difference in EQE compared to that of the control device without the ALD-Al_2O_3 process. Thus, we attribute the observed improvements primarily to the thin Al_2O_3 layer.

In addition to the ALD-Al_2O_3 layer between CZTS and CdS, we replace the intrinsic ZnO in the standard TCO stack with an ALD-Al_2O_3 layer, as shown in **Figure 3**a. An intrinsic ZnO layer (typically sputtered) is commonly used in the CZTS and CIGS solar cells to increase the shunt resistance by blocking shunt or conduction pathways such as pinholes. The ALD-Al_2O_3 process is expected to cover a wider range of shunt pathways, including high aspect ratio and nanometer-scale cracks and voids. Compared to sputtering, the ALD-Al_2O_3 process is expected to cause less surface damage to the CdS layer. In Figure 3b, we examine over 80 devices in order to compare an ITO/ALD-Al_2O_3/CdS stack with the standard ITO/ZnO/CdS stack. We find that an average V_{OC} enhancement of ≈5% is observed when replacing the sputtered ZnO with an ALD-Al_2O_3 layer (Figure 3b). This results in an efficiency improvement of the same magnitude (Figure 3c). The thickness of this Al_2O_3 layer was kept to 0.5 nm to minimize series resistance. Thus, we demonstrate that while the much of the V_{OC}-deficit in CZTS devices likely stems from the disorder in bulk CZTS thin films, these simple methods can improve the average device performance without otherwise modifying CZTS film processing and may be applicable to other systems employing sputtered ZnO buffer layers.

We note that the thicknesses of ALD-Al_2O_3 layer initially deposited onto CZTS as discussed with reference to Figure 2b (e.g., 10 nm) would be significantly too insulating to allow for normal device operation if the layer remained fully intact. The high performance is enabled by significant dissolution of the Al_2O_3 present on the CZTS surface in the NH_4OH-containing

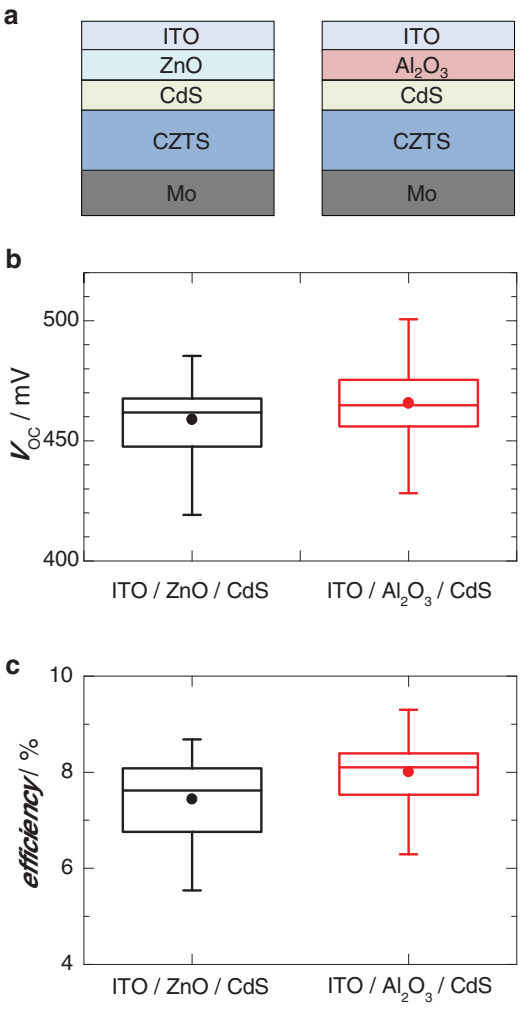

Figure 3. a) Schematic of device structures with ZnO (left, control) and Al_2O_3 (right) layers. b) Box-plot diagram of statistical data of power conversion efficiency and c) V_{OC} values from over 80 devices prepared with a 0.5 nm thick Al_2O_3 layer inserted between CdS and ITO layers (red) and control devices with a standard ITO/ZnO/CdS stack (black). Boxes, circle symbols, and horizontal bars indicate 25/75 percentile, mean, and min/max values, respectively.

chemical bath deposition (CBD) solution, leaving behind predominantly near-surface, grain boundary, and/or pinhole passivation. NH_4OH-containing solutions are known to etch Al_2O_3 thin films, especially at elevated temperatures.[27] The predicted etching of surface Al_2O_3 is supported by measurements of the device series resistance (R_S) with varying Al_2O_3 layer thicknesses deposited both prior to and after the CBD process for CdS layer, as shown in **Figure 4**a. While increasing the Al_2O_3 layer thickness between CdS and ITO above ≈1 nm has a notable effect on the R_S of the solar cell devices, increasing the passivating Al_2O_3 layer thickness up to ≈5 nm between CZTS and CdS does not impact R_S, indicating that the Al_2O_3 layer initially present on the CZTS surface must be thinned during the CBD process.

Figure 4b shows secondary ion mass spectrometry (SIMS) depth profiles of two CZTS solar cell devices prepared with 1 and 5 nm thick ALD-Al_2O_3 layers deposited between the

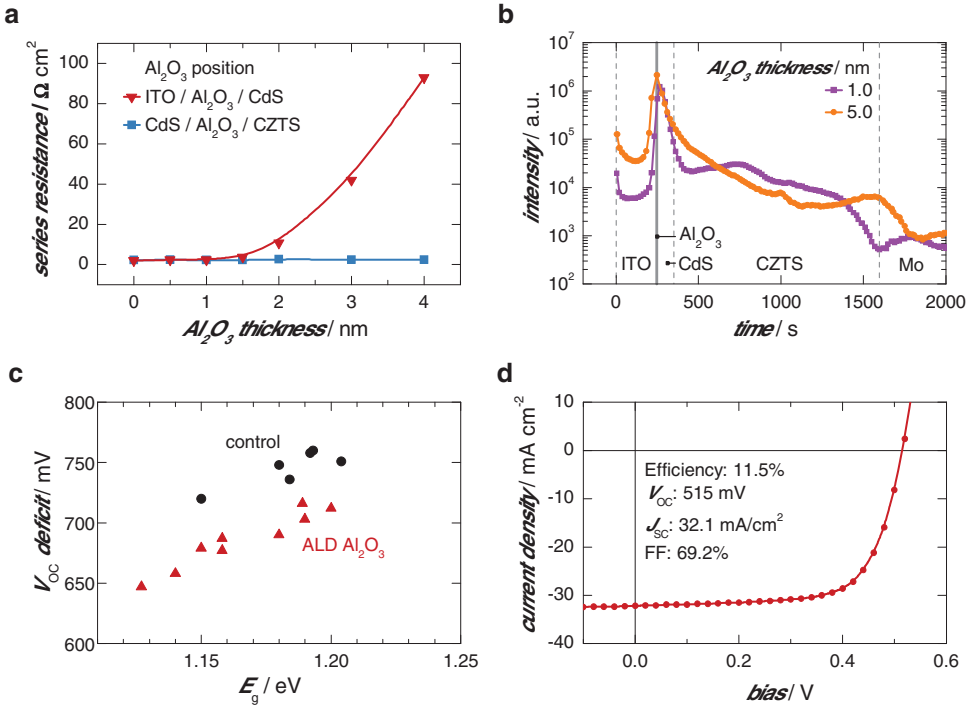

Figure 4. a) SIMS depth profiles of Al element throughout the device stack in samples containing ALD-Al_2O_3 layers on CZTS and CdS surfaces. Purple and orange colored lines indicate the devices with 1 and 5 nm thick Al_2O_3 layers, respectively. b) Series resistance values of CZTS solar cell devices plotted as a function of Al_2O_3 layer thickness for both the passivation technique (on CZTS) and buffer layer (on CdS). c) Plot of the V_{OC}-deficit in the presence (red) and absence (black) of the ALD-Al_2O_3 layer between the CdS and the sputtered ITO layer. d) *J–V* characteristic of the best-performing device with an ALD-Al_2O_3 buffer layers and a MgF_2 anti-reflective coating layer under the 1 Sun (100 mW cm^{-2}, AM1.5G filtered) illumination condition.

CZTS and CdS as well as a 0.5 nm thick layer between CdS and ITO. While a sharp peak of Al is observed between ITO and CdS layers, no visible peak is observed between CdS and CZTS layers, indicating that the Al_2O_3 layers on the top surface of CZTS were largely dissolved during the CBD process. Additionally, the Al signal persists throughout the CZTS layer all the way to the Mo bottom electrode. The temperature of 150 °C used to grow the ALD-Al_2O_3 layer is insufficient to diffuse Al through the bulk of the CZTS layer. Therefore, the presence of Al in the CZTS layer and at the interface between CZTS and Mo layer indicates that the ALD precursor has penetrated into pinholes and/or grain boundaries of CZTS, where it forms an insulating Al_2O_3 layer.

By combining the two approaches of ALD-Al_2O_3 incorporation, we demonstrate a significant reduction in the V_{OC}-deficit, as plotted in Figure 4c. The bandgap of CZTS was estimated by measuring the inflection point of the EQE spectra. Low-bandgap CZTS devices with high Se/(S + Se) ratios show reduced V_{OC}-deficit, consistent with previous reports.[4,28] A significant reduction in V_{OC}-deficit is observed by incorporating ALD-Al_2O_3. Figure 4d shows the photovoltaic properties and the current density versus voltage (*J–V*) characteristics of the best performing device incorporating both types of ALD-Al_2O_3 layers (standard AM1.5G 1 Sun illumination conditions). The device shows a total-area efficiency of 11.5% under 1 Sun AM1.5 global normal spectral irradiance (100 mW cm^{-2}), with an MgF_2 anti-reflection coating. The J_{SC}, V_{OC}, and FF of the device are measured to be 32.1 mA cm^{-2}, 515 mV, and 69.2%, respectively. The estimated bandgap of the device is 1.183 eV with a V_{OC}-deficit of 668 meV.

In summary, we find that CZTS device performance can be improved by passivating or protecting two different interfaces in solution-processed CZTS devices. First, a thin Al_2O_3 layer deposited on top of the CZTS prior to CdS deposition can improve the surface passivation as well as the J_{SC} and the FF. The improved EQE at all wavelengths, and in particular the long-wavelength region, indicates an improvement in collection length possibly stemming from an improved interface. This is further supported by the observation of significantly enhanced PL for CZTS samples treated with only 1 nm of ALD-Al_2O_3 prior to buffer deposition. Additionally, the Al signal persists throughout the film, indicating that this layer may also passivate pinholes and grain boundaries, accounting for the improved FF. The absorber-passivating ALD-Al_2O_3 layer thickness is optimized by accounting for some dissolution during the CBD CdS process. The absorber passivation effect results in a net efficiency enhancement of up to ≈15%. Second, a thin Al_2O_3 layer inserted between the CdS and the TCO can help prevent damage to the CdS during TCO fabrication and consequently improve efficiency up to 5%.

Experimental Section

Solar Cell Fabrication: CZTS thin films were spin-coated onto Mo-coated glass substrates from a hydrazine-based pure solution precursors.[2,29] (Caution: Hydrazine is toxic and highly reactive material and must be handled using appropriate safety equipment to prevent physical contact with either vapor or liquid.) The composition of CZTS thin films was Cu-poor (Cu/(Zn + Sn) ≈ 0.8) and Zn-rich

(Zn/Sn ≈ 1.1) in accordance with the conditions found optimal for high performance. Annealing was carried out on a custom hotplate in a chalcogen overpressure using a temperature above 550 °C. ALD-Al_2O_3 thin films were prepared on the CZTS layers from TMA and H_2O vapor as aluminum and oxygen precursors at a substrate temperature of 150 °C, using a Savannah S100 ALD system (Cambridge NanoTech). The CdS buffer layers were deposited by using chemical bath deposition method. ZnO and ITO thin films were deposited by radio frequency sputtering, followed by Ni-Al bilayer metal contact deposition by e-beam evaporation. MgF_2 anti-reflection coating layers were deposited on the best performing devices by e-beam evaporation. The solar cell device area was defined by mechanical scribing.

Characterization: SIMS depth profiles were acquired using an IMS Wf (Cameca), with a 4 keV Cs^+ primary ion beam while analyzing CsM^+ cluster ions. Photoluminescence measurements were recorded at room temperature using a 15 kHz pulsed 532 nm laser, a monochromator, and an InGaAs photomultiplier tube detector cooled to −80 °C to minimize noise. *J–V* measurements were performed by using a 6 × 6 $in.^2$ beam solar simulator (Newport) equipped with an AM1.5G filter and a Keithley 2400 sourcemeter. The 1 Sun intensity (100 mW cm^{-2}) was calibrated with a Si reference cell, traceable to the National Renewable Energy Laboratory. The EQE was measured by a QEX10 (PV measurement), calibrated by NIST-certified reference Si and Ge photodiodes.

Acknowledgements

Y.S.L. and T.G. contributed equally to this work. The authors thank Dr. D. B. Mitzi, Dr. Yu Luo, Dr. P. D. Antunez, Dr. Yu Zhu, R. Ferlita, M. Spector, and C. Sturdevant for helpful discussions and experimental support. The work was conducted as part of a joint development project between Tokyo Ohka Kogyo Co., Ltd., Solar Frontier K. K., and IBM Corporation.

Received: January 28, 2016
Revised: March 7, 2016
Published online: April 26, 2016

[1] D. B. Mitzi, O. Gunawan, T. K. Todorov, D. A. R. Barkhouse, *Philos. Trans. R. Soc., A* **2013**, *371*, 20110432.
[2] W. Wang, M. T. Winkler, O. Gunawan, T. Gokmen, T. K. Todorov, Y. Zhu, D. B. Mitzi, *Adv. Energy Mater.* **2014**, *4*, 1301465.
[3] Y. S. Lee, T. Gershon, O. Gunawan, T. K. Todorov, T. Gokmen, Y. Virgus, S. Guha, *Adv. Energy Mater.* **2015**, *5*, 1401372.
[4] T. Gokmen, O. Gunawan, T. K. Todorov, D. B. Mitzi, *Appl. Phys. Lett.* **2013**, *103*, 103506.
[5] M. L. Huang, Y. C. Chang, C. H. Chang, Y. J. Lee, P. Chang, J. Kwo, T. B. Wu, M. Hong, *Appl. Phys. Lett.* **2005**, *87*, 252104.
[6] W.-W. Hsu, J. Y. Chen, T.-H. Cheng, S. C. Lu, W.-S. Ho, Y.-Y. Chen, Y.-J. Chien, C. W. Liu, *Appl. Phys. Lett.* **2012**, *100*, 023508.
[7] J. R. Bakke, K. L. Pickrahn, T. P. Brennan, S. F. Bent, *Nanoscale* **2011**, *3*, 3482.
[8] M. Werner, C. Sutter-Fella, H. Hagendorfer, Y. Romanyuk, A. Tiwari, *Phys. Status Solidi A* **2015**, *212*, 116.
[9] C. Ferekides, U. Balasubramanian, R. Mamazza, V. Viswanathan, H. Zhao, D. Morel, *Sol. Energy* **2004**, *77*, 823.
[10] O. Kunz, J. Wong, J. Janssens, J. Bauer, O. Breitenstein, A. Aberle, *Prog. Photovoltaics* **2009**, *17*, 35.
[11] J. M. Ball, M. M. Lee, A. Hey, H. J. Snaith, *Energy Environ. Sci.* **2013**, *6*, 1739.
[12] B. G. Mendis, M. C. Goodman, J. D. Major, A. A. Taylor, K. Durose, D. P. Halliday, *J. Appl. Phys.* **2012**, *112*, 124508.
[13] W. Li, J. Chen, C. Yan, X. Hao, *J. Alloys Compd.* **2015**, *632*, 178.
[14] M. Buffiere, G. Brammertz, A.-A. El Mel, N. Lenaers, Y. Ren, A. E. Zaghi, Y. Mols, C. Koeble, J. Vleugels, M. Meuris, presented at *Proc. 39th IEEE Photovoltaic Specialists Conf. (PVSC)*, Tampa, FL, June **2013**.
[15] A. Redinger, M. Mousel, M. H. Wolter, N. Valle, S. Siebentritt, *Thin Solid Films* **2013**, *535*, 291.
[16] H. Zhou, T.-B. Song, W.-C. Hsu, S. Luo, S. Ye, H.-S. Duan, C.-J. Hsu, W. Yang, Y. Yang, *J. Am. Chem. Soc.* **2013**, *135*, 15998.
[17] T. Gershon, B. Shin, N. Bojarczuk, M. Hopstaken, D. B. Mitzi, S. Guha, *Adv. Energy Mater.* **2015**, *5*, 1400849.
[18] R. Haight, X. Shao, W. Wang, D. B. Mitzi, *Appl. Phys. Lett.* **2014**, *104*, 033902.
[19] L. Kronik, D. Cahen, H. W. Schock, *Adv. Mater.* **1998**, *10*, 31.
[20] B. Vermang, Y. Ren, O. Donzel-Gargand, C. Frisk, J. Joel, P. Salome, J. Borme, S. Sadewasser, C. Platzer-Bjorkman, M. Edoff, *IEEE J. Photovoltaics* **2016**, *6*, 332.
[21] N. Naghavi, D. Abou-Ras, N. Allsop, N. Barreau, S. Bücheler, A. Ennaoui, C. H. Fischer, C. Guillen, D. Hariskos, J. Herrero, *Prog. Photovoltaics* **2010**, *18*, 411.
[22] T. Nakada, K. Furumi, A. Kunioka, *IEEE Trans. Electron Devices* **1999**, *46*, 2093.
[23] K. Sardashti, R. Haight, T. Gokmen, W. Wang, L.-Y. Chang, D. B. Mitzi, A. C. Kummel, *Adv. Energy Mater.* **2015**, *5*, 1402180.
[24] J.-H. Kim, S.-Y. Choi, M. Choi, T. Gershon, Y. S. Lee, W. Wang, B. Shin, S.-Y. Chung, *Adv. Energy Mater.* **2016**, *6*, 1501902.
[25] J. J. Scragg, L. Choubrac, A. Lafond, T. Ericson, C. Platzer-Björkman, *Appl. Phys. Lett.* **2014**, *104*, 041911.
[26] S. Siebentritt, G. Rey, A. Finger, D. Regesch, J. Sendler, T. P. Weiss, T. Bertram, *Sol. Energy Mater. Sol. Cells* DOI: 10.1016/j.solmat.2015.10.017.
[27] J. Oh, J. Myoung, J. S. Bae, S. Lim, *J. Electrochem. Soc.* **2011**, *158*, D217.
[28] J. Kim, H. Hiroi, T. K. Todorov, O. Gunawan, M. Kuwahara, T. Gokmen, D. Nair, M. Hopstaken, B. Shin, Y. S. Lee, W. Wang, H. Sugimoto, D. B. Mitzi, *Adv. Mater.* **2014**, *26*, 7427.
[29] T. Todorov, H. Sugimoto, O. Gunawan, T. Gokmen, D. B. Mitzi, *IEEE J. Photovoltaics* **2014**, *4*, 483.

